Electronic Supplementary Material (ESI) for ChemComm.

Hollow Ag/AgCl Nanoelectrode for Single-Cell Chloride Detection

Tian-Yang Zhang,[a] Fang-Qing Liu,[a] Zheng Li,[a] Yi-Tong Xu,[a] Wei-Wei Zhao,*[a] Hong-Yuan Chen,[a] and Jing-Juan Xu*[a]

Key Laboratory of Analytical Chemistry for Life Science, School of Chemistry and Chemical Engineering, Nanjing University, Nanjing 210023, China. E-mail: zww@nju.edu.cn; xujj@nju.edu.cn

Table of contents

1. Experimental Section

Reagents and Materials. Potassium sulfate (K_2SO_4), sodium sulfate (Na_2SO_4), magnesium chloride ($MgCl_2$), glycerin, calcium chloride anhydrous ($CaCl_2$), sodium chloride (NaCl), potassium fluoride (KF), potassium bromide (KBr) potassium iodide (KI), hydrogen peroxide (H_2O_2), dichloromethane (CH_2Cl_2), cysteine (L-Cys), glutathione (GSH), sodium nitrite ($NaNO_2$), N,N-Dimethylformamide (DMF), polyacrylonitrile (PAN), sodium nitrate ($NaNO_3$), sodium bisulfite ($NaHSO_3$), sodium sulfide (Na_2S), 2-[4-(2-hydroxyethyl) piperazin-1-yl] ethane sulfonic acid (HEPES) and other reagents were purchased from Sinopharm Co., Ltd. Dimethyl sulfoxide (DMSO) and resveratrol were purchased from Sigma-Aldrich (St.Louis, MO, USA) (Sigma). Apiezon wax (Type W) was purchased from APIEZON (M&I Materials Ltd, United Kingdom). BzATP was obtained from Target Mol Co., Ltd. (Shanghai, China). Silver target was obtained from ZhongNuo Advanced Material (Beijing Technology Co., Ltd), All aqueous solutions were prepared in deionized water (Millipore) with a resistivity of 18.2 MΩ*cm and silver wires (Φ 0.2 mm) were obtained from Sinopharm Chemical Reagent Co., Ltd. (Shanghai, China). 1× PBS (phosphate buffered solution, 10 mM, pH 7.2 - 7.4), 2.2 mM EDTA solution containing 0.25% trypsin, Hoechst 33342 and propidium iodide (PI) were purchased from Keygenbio Co., Ltd. (Nanjing, China). Fetal bovine serum (FBS) was purchased from Gibco (USA). Resveratrol was purchased from Shanghai Aladdin Bio-Chem Technology Co., LTD.

Experimental Setup and Data Acquisition. All current measurements were recorded with CHI-760e electrochemical workstation (CH Instruments Ins, China), and the workstation was operated in conjunction with the CHI-200B micro-current signal amplifier to stably collect current signals. A three-electrode system was introduced for testing with the prepared electrochemical microelectrode as the working electrode, and $Hg/HgSO_4$ as the reference electrode and counter electrode. The potential-time (V-t) curves were recorded at a voltage of 0 V bias with the sampling interval of 0.1 s and the sampling time of 45 s. The V-t curve recordings were analyzed by CHI software and plotted with OriginLab 8.5. Intracellular detection experiments were performed in virtue of a three-dimensional TransferMan 4r micromanipulator (Eppendorf Instrument, USA) equipped with an inverted microscope (IX73, TH4-200, U-HGLGPS, Olympus Corporation, Japan; Ti2-E, Nikon, Japan) for the precise control of the nanopipette towards inserting into single cells under observation. The nanotool was fixed to the micromanipulator with a holder (Axon Instruments, Union City, CA) connected to an Axopatch Multiclamp 700B low-noise amplifier (Axon Instruments, Union City, CA). Multiclamp 700B amplifier in gap-free mode with the Digidata 1550 digitizer (Molecular Devices, Sunnyvale, CA) and a PC equipped with pCLAMP10.5 software (Molecular Devices) was used to assist the baseline current monitoring for better operational control. Scanning electron microscopic (SEM) characterization was performed on a JSM-7800F Instrument (JEOL, Japan).

Fabrication of the Nanopipette. To functionalize the nanopipettes, the fabrication and selection of tip was achieved in following steps. Borosilicate glass capillaries (O.D.: 1.0 mm, I.D.: 0.58mm; 10 cm length) were purchased from Sutter Instrument and were fabricated by a P-2000 pipette puller (Sutter Instrument, Novato, CA, USA) with two-line program containing the following parameters: Line 1: Heat = 350, Fil = 3, Vel = 40, Del = 200, Pull = ; Line 2: Heat = 340, Fil = 3, Vel = 37, Del =170, Pull = 180. To ensure the reproducibility of nanotip geometry, the variation of nanopipette pulling time was controlled within 0.2 second.

Sliver Layer Sputtering. The as-pulled capillaries were coated with a sliver (Ag) layer through magnetron sputtering method. Magnetron Sputtering Equipment and the sputtering targets of Ag and Titanium (Ti) were purchased from ZhongNuo Advanced Material (Beijing) Technology Co., Ltd. The laser-pulled nanopipettes were fixed on the self-made bench bed with a consistently constant exposed length, following with a specific operation parameter with 50 s under Ti default mode for Ti sputtering. Then same step was applied with 440s under Ag default mode for Ag sputtering.

Preparation of the cell lysate. In addition, to exclude other side effects, the nanotool was sequentially immersed into the cell lysate (100 cells mL^{-1}) for 10 min and then tested for three repeated times. As shown in Figure S5. To preparation of the cell lysate (100 cells mL^{-1}), MCF-7 cells were digested using trypsin enzyme-digesting and then centrifuged with 1000 rpm, 5 min. Afterwards, the sediment was diluted with 1mL HEPES (10 mM) and the cell density was then calculated via counters II (Life, the USA). Then the cell lysate was obtained by treating the diluted cell solution n at 0 °C using ultrasonic cell crusher with noise isolating chamber (Anxiu, China), which was set to the following program: 35% power, 2 min, rod 6, 5 s ultrasound and 5s pause. Finally, the product was diluted to the corresponding concentration.

Cell Culture. MCF-7 cells were purchased from KeyGen BioTECH (China) and then were cultured in DMEM (Gibaco, USA) containing 10% fetal bovine serum and antibiotics (penicillin and streptomycin). Afterwards, the culture environment was maintained at 37 °C in 5% CO_2 / 95% air.

Cells Vitality Measurement. To monitor the changes of cell vitality after intracellular drug delivery, Hoechst 33342 was firstly used to stain the MCF-7 cells, which was carried out with the following experimental steps. For control test, after

the cell insertion and delivery by the nanotool, no significant damage of cell vitality was observed. The propidium iodide (PI) membrane impenetrable and Hoechst 33342 dyes were used to study the cell vitality according to the instructions.

For Hoechst 33342 dye staining, MCF-7 cells were rinsed three times with 1× PBS and the nucleus of which were stained with 500 µL Hoechst 33342 for 10 min, and then rinsed three times with 1× PBS again for adding the testing solution. The normal cell nucleuses could be slightly stained and show low blue fluorescence, However the dead cells could show brighter blue fluorescence.

As to PI dye staining, MCF-7 cells were rinsed three times with 1× PBS and stained with 1 mL PI for 30 min, then prepared for the following experiment. PI dye has no membrane impermeability with living cells, but can stain the dead cells to show red fluorescence.

In-Situ Delivery of FITC. The detailed steps of intracellular analysis were described below: The nanotool with 1× PBS backfilled was anchored on the holder of the three-dimensional MP-225 micromanipulator equipped on an inverted microscope, and the gap-free mode function of pCLAMP10.5 software was introduced to assist real-time monitoring of the changes in baseline current. The cavity of the nanotool was inserted with the Ag/AgCl electrode on the patch clamp holder, while another reference Ag/AgCl electrode was stationed nearby in the surrounding medium bath (1× PBS). With the help of the MP-225 micromanipulator, the nanotool could perform a submicron movement on all three axes towards precise position control. The cavity of the nanotool was backfilled with FITC dye for the verification of the intracellular delivery process. Specifically, 6.5 µL of 10 mM FITC was backfilled into the nanopipette, and then the nanotool was fixed on the patch clamp holder. A voltage bias of 0 mV was applied before penetration into the cell. After insertion of the nanotip, the nanotool was allowed to stand for 1 min with a positive bias of +1.0 V to inject FITC into the cytoplasm through electroosmosis. After that, the bias voltage was changed to 0 V, and the nanotool was quickly withdrawn from the single-cells. Fluorescence images of the single MCF-7 cell with the intracellular delivery were collected as shown in Figure S6.

Intracellular Delivery and Detection. The nanotool was backfilled with drug and used for intracellular in-situ delivery and stimulation experiments.

For BzATP, 100 µM drug (solved in 10 mM HEPES buffer, pH 7.4, containing 10 mM KCl for the balance of extracellular chloridion) was backfilled into the nanotool, and then followed the same steps by in-situ delivery of FITC section (different electroosmosis time) with CHI760e used to record the corresponding signal. Afterward, for intracellular detection, the MCF-7 cells with the incubation of BzATP was carried out for different time until cells apoptosis (confirmed by Hoechst 33342 dye fluorescence), and the corresponding signal was monitored via CHI760e in open circuit potential mode in the step of Experimental Setup and Data Acquisition.

As to the resveratrol, nanotool was backfilled with 10 mM HEPES containing 100 µM resveratrol, 2% DMSO and 98% 10 mM KCl, intracellular detection of MCF-7 cells with or without drug treatment followed the steps as similar to the previous paragraph description.

The delivery of resveratrol for 1 min +1.0 V electroosmosis was set as the example, which is shown in Figure S7.

2. Typical Application of Nanopipette-Derived "Metallic Redox Indicators" for Faradic Detection

Table S1. The application of nanopipette-derived "metallic redox indicators" for Faradic detection.

Experiment method	Descriptions	Applications of analysis	Ref.
Well-shaped platinized nanoprobes	Fabricating platinized nanoelectrodes under atomic force microscope (AFM) control.	Detecting ROS and RNS.	1
Scanning electrochemical microscopy (SECM)	Well-shaped platinized carbon nanoelectrodes as SECM tips for precise detection.	The detection of ROS/RNS related parameters in biological systems.	2
A novel asymmetric nanopore electrode (ANE)	An asymmetric nanopore electrode-based amplification mechanism.	Real-time monitoring of NADH in a living cell.	3
An electrochemical detector and separator	The analysis of protein activity within targeted cellular compartments at subcellular resolution.	Separating a single lysosome from the living cell and related detection.	4
Platinized nanowire electrodes (Pt-NWEs)	Nanoelectrochemical monitoring of intracellular ROS/RNS at the single cell level.	Monitoring ROS/RNS effluxes on from individual phagolysosomes.	5
Scanning electrochemical microscopy (SECM)	Platinized carbon nanoelectrodes combined with a four-step chronoamperometric method.	Monitoring the time-dependent concentrations of the four primary ROS/RNS in individual phagolysosomes.	6
Dual-functional photocathodic single-cell nanotool	Direct electroosmotic intracellular drug delivery and evaluation of oxidative stress.	Precise assessment of specific drug effects.	7
Highly robust aptamer-based microsensor	Interface aptamers with implantable electrodes for in vivo sensing.	In vivo sensing of dopamine.	8

3. Characterization of Silver/Silver-Chloride Layer

To study the surface morphology of the silver/silver-chloride layer, the identical preparation was constructed upon a plane surface for scanning atomic force microscope (AFM) characterization. As shown in Figure S1a, Ag nanoparticles distributed evenly on the surface with the size about 3 nm. After chlorination, AgCl nanoparticles distributed evenly on the surface with the size about 90 nm, as shown in Figure S1b, indicating the successful construction of silver/silver-chloride layer.

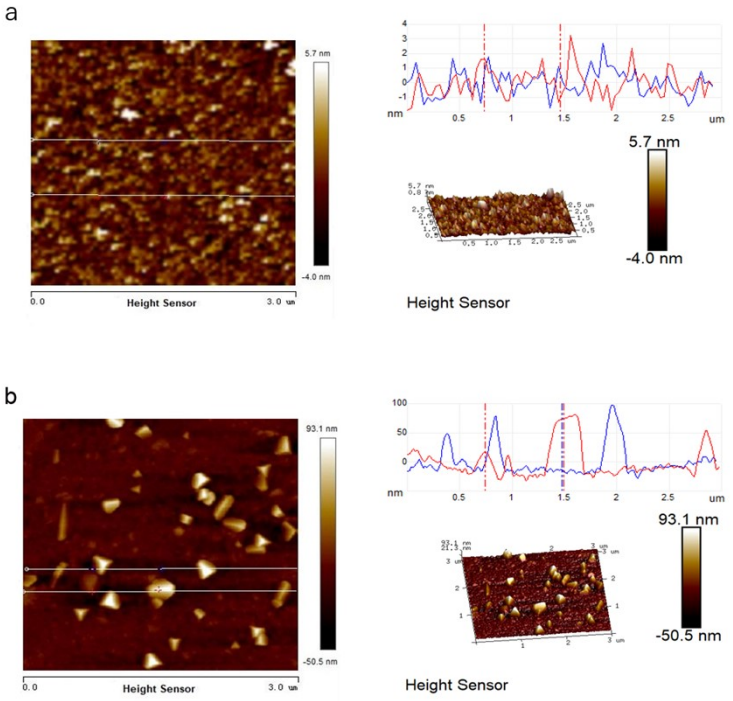

Figure S1. The AFM images of sputtering layer. Two-dimensional image (left), and height profile (upper right) and topographic image (bottom right) of a) pristine silver and b) silver/silver-chloride layer.

EIS was used as another effective analytical tools to confirm the surface modification process (Figure S2).

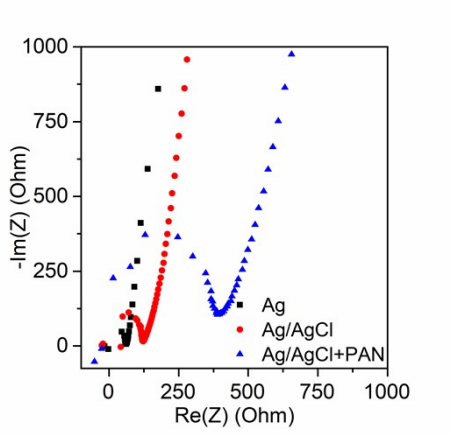

Figure S2. The nyquist plots of electrode after each fabrication step.

4. Anti-interference Tests

As shown in Figure S3, the potential signal was monitored under 10 mM HEPES buffer containing 0.1 M chloridion for 1000 s and there was no noticeable change, indicating the stability of nanotool.

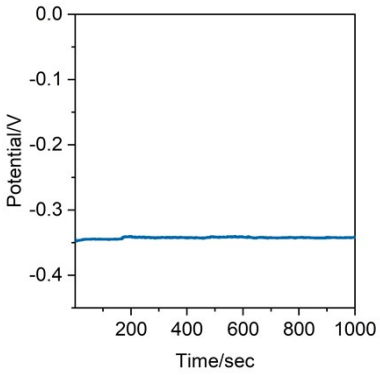

Figure S3. The stability of the nanotool. The experiment was performed in 10 mM HEPES buffer containing 0.1 M chloridion for 1000 s.

To exclude the possible effect of the pH variation, the nanotool was tested in 10 mM HEPES buffer containing 0.1 M chloride with different pH of 6.4, 7.4 and 8.0. As shown in Figure S4, the identical signals indicated that the pH had no effect on the response of the nanotool.[9, 10]

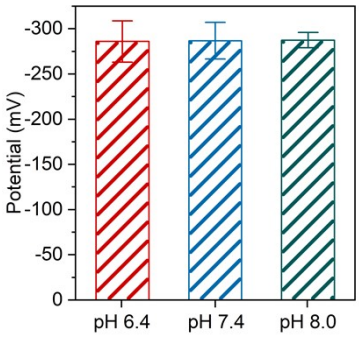

Figure S4. The possible effect of the pH variation. The pH values of 6.4, 7.4 and 8.0 in 10 mM HEPES buffer containing 10 mM chloridion were chosen.

To study the possible adsorption, the nanotool was sequentially immersed into the cell lysate for 15 min and then tested. As shown in Figure S5, the nearly identical signals indicated there was little adsorption on the nanotool.

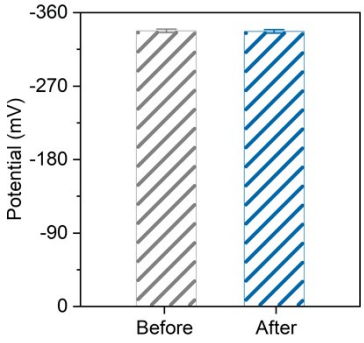

Figure S5. The possible adsorption of nanopipette. Adsorption tests were sequentially performed after immersing the nanotool in cell lysate for 15 min.

5. Cell Viability Measurements

Fluorescein isothiocyanate (FITC) is regarded as small molecules as the same with the drug and was chosen for validating the successful intracellular delivery of the drug. As shown in Figure S6, the electroosmotic cytosolic delivery of FITC was carried out into a single MCF-7 cell. The green fluorescence appeared inside the cell after the electroosmotic delivery at +1.0 V for 1 min indicated the successful intracellular delivery.

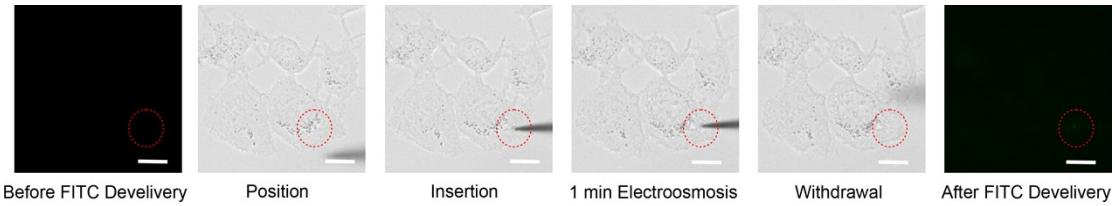

Figure S6. Bright-field and fluorescence images showing the delivery of FITC into a single MCF-7 cell via +1.0 V electroosmosis for 1 min. Scale bars: 25 µm.

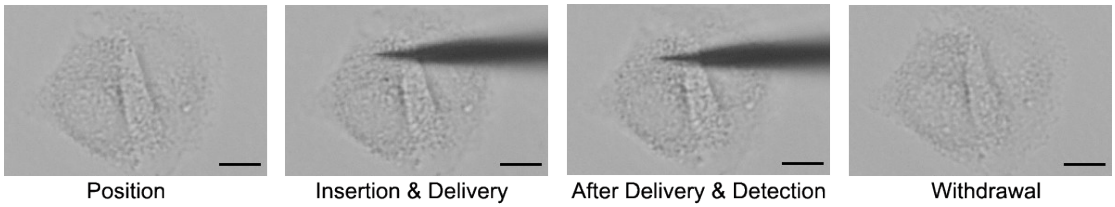

Figure S7. Bright-field images showing the delivery of resveratrol into a single MCF-7 cell via +1.0 V electroosmosis for 1 min. Scale bars: 5 µm.

Propidium iodide (PI), the membrane impermeable dye, was used to stain the MCF-7 cells to verify the membrane integrity of the cell after insertion. PI dye has no membrane impermeability in living cells, but can stain the dead cells to show red fluorescence. The fluorescence micrographs of PI stained MCF-7 cells before and after penetration and withdrawal of the nanotool were shown in Figure S8. After the 15 min of penetration and 15 min of withdrawal, no red fluorescence was observed, indicating the good membrane integrity of the targeted MCF-7 after the penetration of the nanotool.

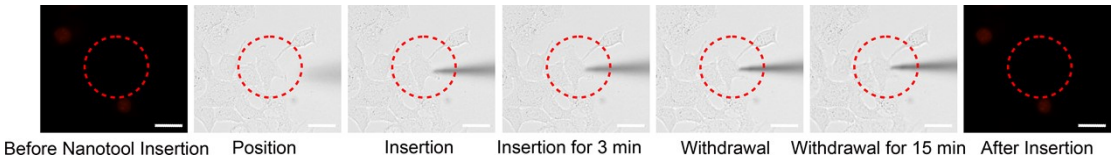

Figure S8. Bright and fluorescent images of PI stained cells before and after the penetration and withdrawal of the nanopipette. Scale bars: 25 µm.

To study the cell viability of the cell after insertion, Hoechst 33342 was used to stain the MCF-7 cells. This dye has a certain membrane permeability and the normal cell nucleus could be slightly stained and show low blue fluorescence, but the dead cells could show brighter blue fluorescence. The fluorescence micrograph of Hoechst 33342 stained MCF-7 cells before penetration and after withdrawal of the nanotool were shown in Figure S9. After the 15 min of penetration and 15 min of withdrawal, no change of the fluorescence could be observed, indicating the good cell viability of the targeted MCF-7 cell after the penetration of the nanotool.

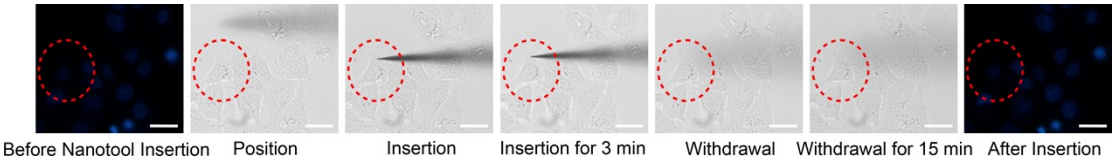

Figure S9. Bright and fluorescent images of Hoechst 33342 stained cells before and after the penetration and withdrawal of the nanopipette. Scale bars: 25 µm.

6. In Situ Intracellular Drug Delivery and Chloridion Detection

As shown in Figure S10a-S10b, the same drug delivery condition was respectively carried out at 1 min and 2 min for two drugs under +1 V. With the increasing of electroosmotic delivery time, the potential declined with time and the equilibrium time decreased to 90 min and 20 min for resveratrol and BzATP respectively.

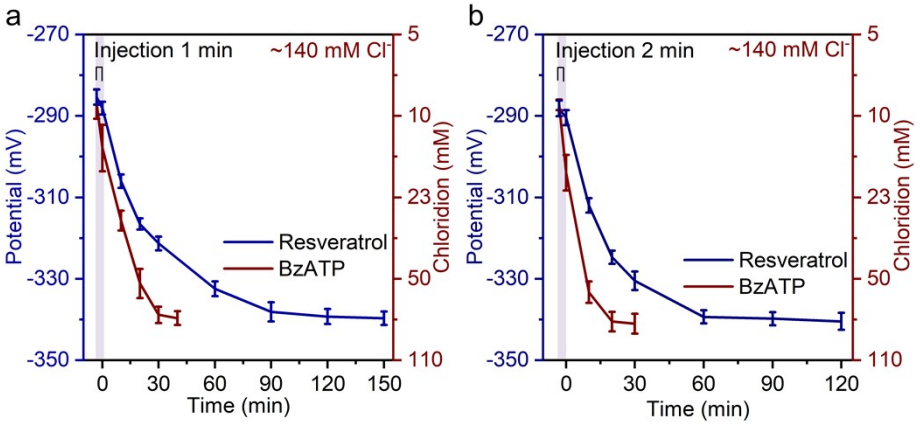

Figure S10. The evolution of recorded potential and corresponding intracellular chloride level MCF-7 cells treated by electroosmotic delivery of 100 μM resveratrol and BzATP under +1 V with extracellular chorion of ~140 mM for a) 1 min and b) 2 min. Error bars represent standard deviations from 10 independent detections.

7. Cell Viability as Indicated by Fluorescence

The cell apoptosis was studied with the development of 100 μM resveratrol treatment as stained by Hoechest 33342. Before the experiment, the concentration of extracellular chlorion was set as ~140 mM.

As shown in Figure S11-S13, with the increase of delivery time, the process of cell apoptosis caused by resveratrol accelerated. In addition, the similar phenomenon was observed in the electroosmotic delivery of 100 μM BzATP, as shown in Figure S14-S16). While the control experiment showed that the electroosmotic delivery would not cause the cell apoptosis after MCF-7 cells treated by 10 mM KCl and 10 mM HEPES (drug solvent) using electroosmotic delivery under +1 V for 3 min with extracellular chlorion of ~140 mM, as shown in Figure S17.

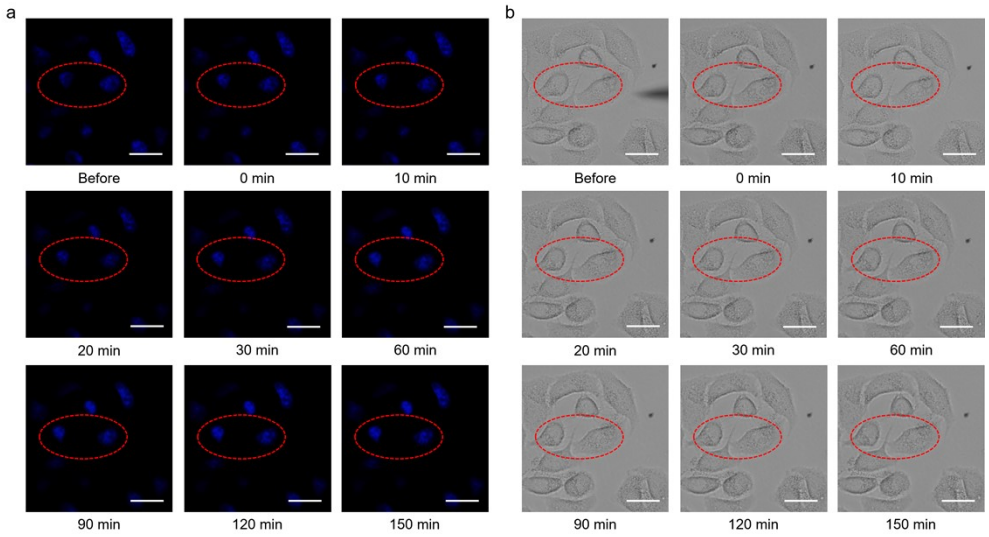

Figure S11. a) Fluorescent images and b) bright-field images of MCF-7 cells treated by 100 μM resveratrol using electroosmotic delivery under +1 V for 1 min with extracellular chlorion of ~140 mM. Scale bars: 25 μm.

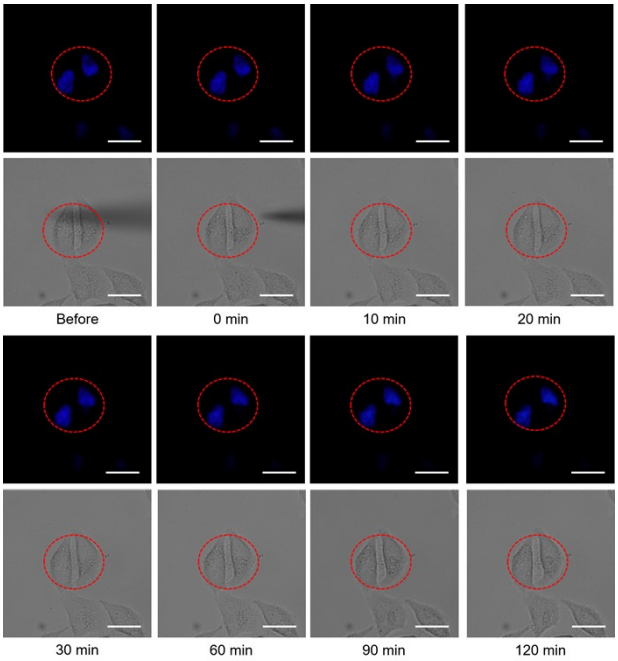

Figure S12. a) Fluorescent images and b) bright-field images of MCF-7 cells treated by 100 μM resveratrol using electroosmotic delivery under +1 V for 2 min with extracellular chloride of ~140 mM. Scale bars: 25 μm.

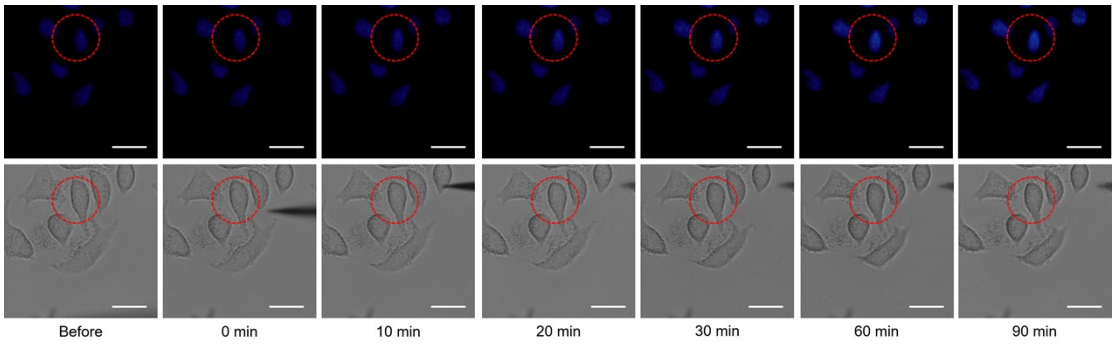

Figure S13. a) Fluorescent images and b) bright-field images of MCF-7 cells treated by 100 µM resveratrol using electroosmotic delivery under +1 V for 3 min with extracellular chloride of ~140 mM. Scale bars: 25 µm.

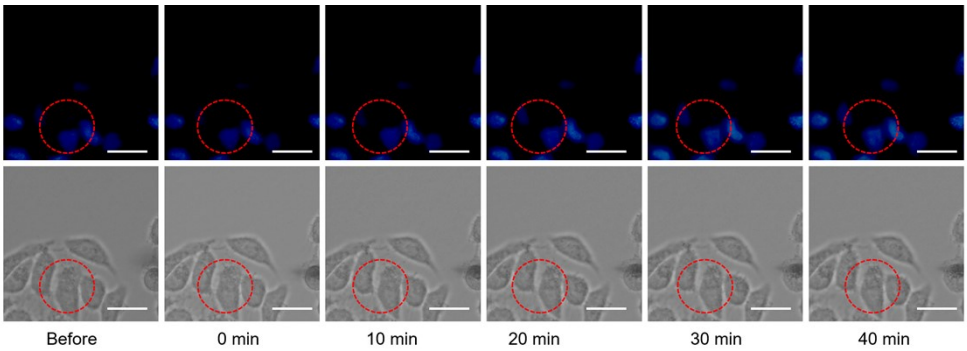

Figure S14. a) Fluorescent images and b) bright-field images of MCF-7 cells treated by 100 µM BzATP using electroosmotic delivery under +1 V for 1 min with extracellular chloride of ~140 mM. Scale bars: 25 µm.

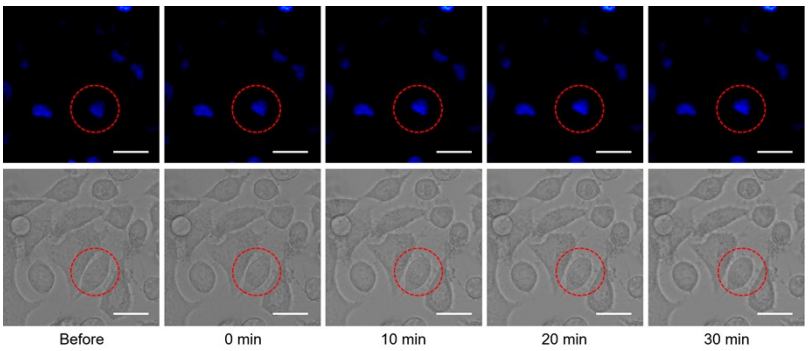

Figure S15. a) Fluorescent images and b) bright-field images of MCF-7 cells treated by 100 µM BzATP using electroosmotic delivery under +1 V for 2 min with extracellular chloride of ~140 mM. Scale bars: 25 µm.

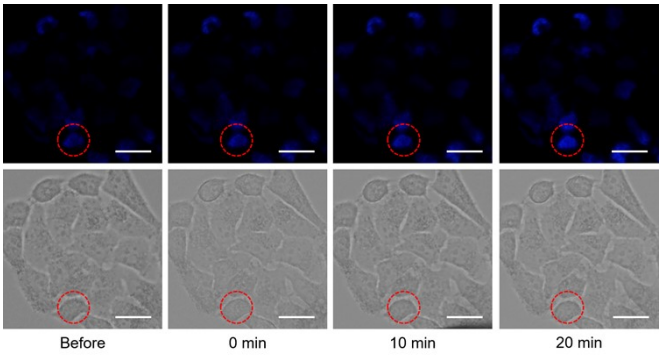

Figure S16. a) Dark-field and b) bright-field images of MCF-7 cells treated by 100 μM BzATP using electroosmotic delivery under +1 V for 3 min with extracellular chloride of ~140 mM. Scale bars: 25 μm.

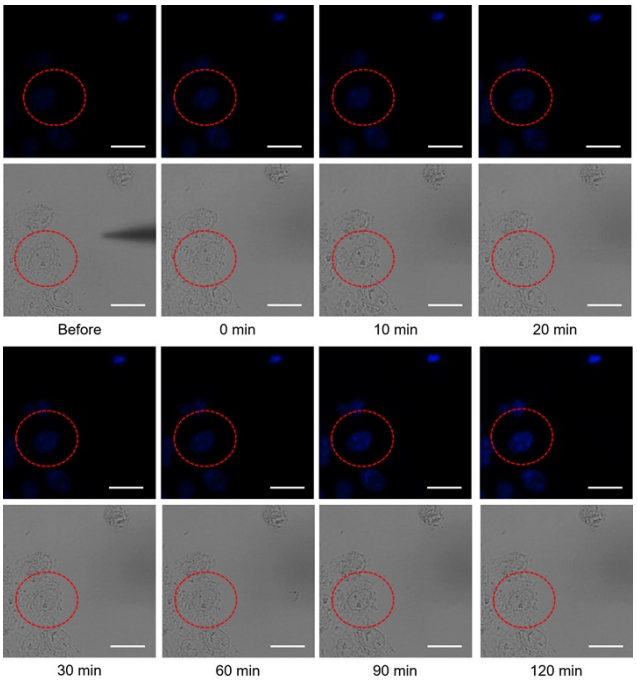

Figure S17. a) Fluorescent images and b) bright-field images of MCF-7 cells treated by 10 mM KCl and 10 mM HEPES (drug solvent) using electroosmotic delivery under +1 V for 3 min with extracellular chloride of ~140 mM. Scale bars: 25 μm.

Then, similarly, the concentration of extracellular chloride was set as 10 mM, and MCF-7 cells were respectively treated with 100 μM resveratrol and 100 μM BzATP. The experiment was conducted with electroosmotic delivery under +1 V for 3 min. Noted that, the cell viability was monitored via Hoechest 33342 staining. As shown in Figure S18, after the addition of resveratrol, the fluorescence increased, indicating the occurrence of the cell apoptosis. As shown in Figure S19, there was no change in fluorescence of cells, which indicated that the cell apoptosis did not occur after the treatment of BzATP. Meanwhile, the control experiment also indicated that the electroosmotic delivery would not cause cell apoptosis after MCF-7 cells treated by 10 mM KCl and 10 mM HEPES (drug solvent) using electroosmotic delivery under +1 V for 3 min with extracellular chorion of ~10 mM (Figure S20).

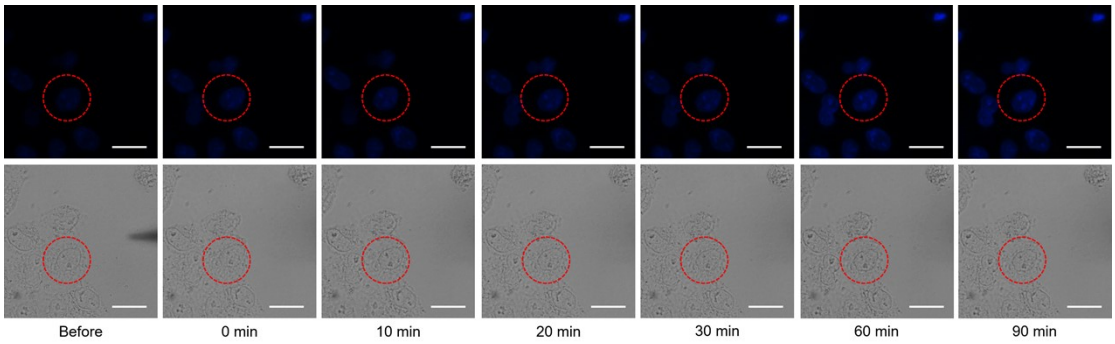

Figure S18. a) Dark-field and b) bright-field images of MCF-7 cells treated by 100 µM resveratrol using electroosmotic delivery under +1 V for 3 min with extracellular chloride of ~10 mM. Scale bars: 25 µm.

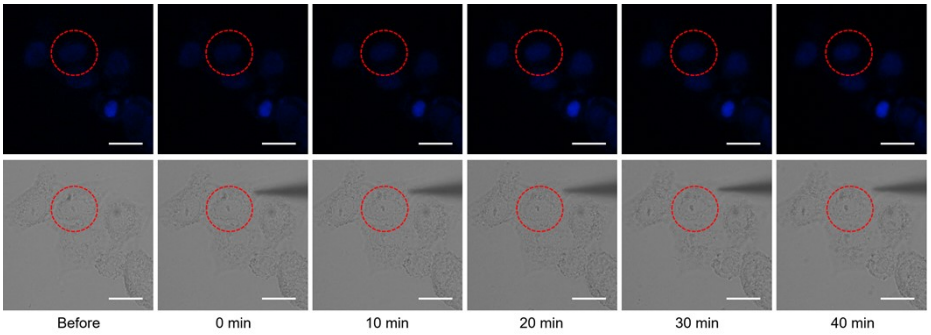

Figure S19. a) Dark-field and b) bright-field images of MCF-7 cells treated by 100 µM BzATP using electroosmotic delivery under +1 V for 3 min with extracellular chloride set as ~10 mM. Scale bars: 25 µm.

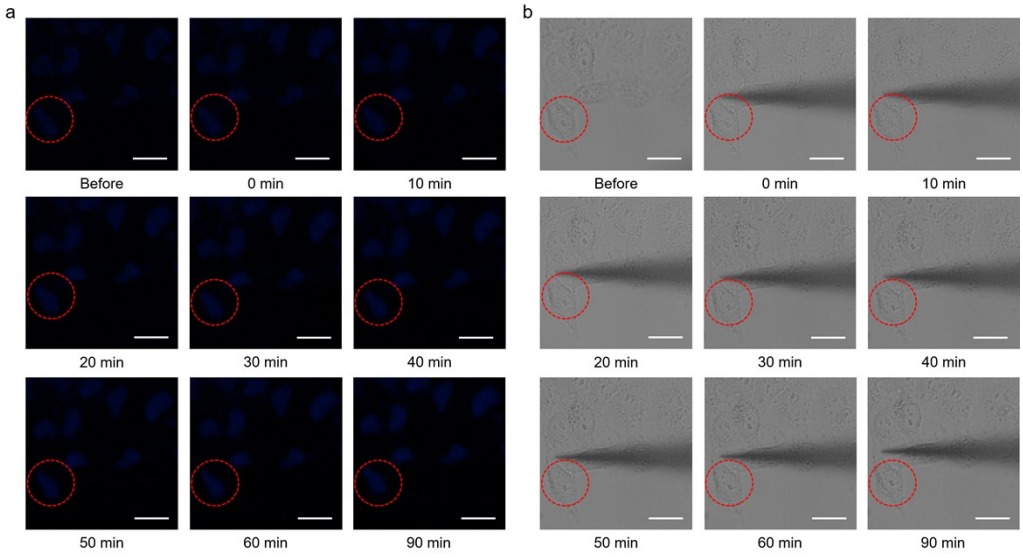

Figure S20. a) Dark-field and b) bright-field images of MCF-7 cells treated by 10 mM KCl and 10 mM HEPES (drug solvent) using electroosmotic delivery under +1 V for 3 min with extracellular chloride of ~10 mM. Scale bars: 25 µm

It is observed that resveratrol and BzATP both resulted in increased chloride concentration and apoptosis while the increase of chloride concentration was more rapid in the BzATP group under normal extracellular chloride concentration (1x PBS). This is due to BzATP is a chloride influx drug, which leads to apoptosis at normal extracellular chloride concentrations. On the other hand, the increase in chloride concentration in resveratrol was attributed to a change in the

permeability of the cell membrane due to apoptosis, resulting in an increase in the concentration of intracellular ions. In the case of low extracellular chloride concentration (comparable to the intracellular chloride concentration), BzATP could still cause the obvious chorion influx, but didn't result in apoptosis. Whereas resveratrol could hardly induce alternation of the intracellular chloridion level. This was due to the comparable intracellular and extracellular chloridion. Low chloridion can prevent apoptosis caused by BzATP, while resveratrol cannot, indicating the different roles of the two drugs in the signal transduction pathways of the treated cells.

In summary, under normal chloride concentration (1x PBS, ~140 mM), BzATP and resveratrol could induce apoptosis. (Figure S11-S16) However, low chloride concentration would decrease chorion influx influence from chloride influx drug, BzATP, so as to avoid apoptosis (Figure S18), whereas resveratrol still arises apoptosis under the same condition (Figure S18). These results indicated that the extracellular chloride concentration could only affect BzATP effect, for their different induce-apoptosis mechanisms. What's more, with the longer time drug delivery (1-3 min, Figure S11-S13 and Figure S14-S16), the onset time of drug is shorter.

8. Typical Application of anticancer methods for drug delivery.

Table S2. The application of anticancer methods for drug delivery.

Drug	Application	Drug delivery method	Onset time	Ref.
Resveratrol	MDA-MB-231 cell (human metastatic breast cancer cells)	Incubated with 200 μM resveratrol.	12 h	[11]
Resveratrol	MCF-7 cell (human non-metastatic breast cancer cells)	Incubated with 100 μg/ml resveratrol.	8 h	[12]
Resveratrol	MCF-7 cell (human non-metastatic breast cancer cells); HepG2 cells (human hepatocellular liver carcinoma cells)	Incubated with 100 μM resveratrol.	6 h	[13]
Resveratrol	HCPC I cell (oral squamous cell carcinoma cell)	Incubated with 100 μM cyclodextrins coated resveratrol.	72 h	[14]
BzATP	DT 40 cell (lymphoma cells)	Incubated with 100 mM BzATP.	90 min	[15]
BzATP	CaSki cell (cervical carcinoma epithelial cells)	Incubated with 100 uM BzATP	9 h	[16]

9. Typical methods of cloridion detection.

Table S3. The methods of cloridion detection.

Detection method	Applications of analysis	Advantage	Ref.
A dual-labeled fluorescent probe by conjugation of the chloride-sensitive 6-methoxyquinoline and chloride-insensitive. tetramethylrhodamine to the zymosan particles.	Free chloride ion concentrations within the phagolysosomal compartment of human neutrophils.	Realize the detection of phagolysosomal compartment of human neutrophils	[17]
Chloride-sensitive fluorescent proteins based on fluorescent proton-pumping rhodopsin.	E. coli treated with various sodium chloride concentration.	A reversible, ratiometric fluorescent sensor for chloride which has a little background fluorescence.	[18]
Two-photon imaging sensor constructed by fusion of an ion-sensitive GFP (E2 GFP) with a red fluorescent protein (LSSmKate2).	The mouse cortex during hypercapnia and seizure activity at the single-cell level.	Dynamic and simultaneous monitoring of intraneuronal Cl^- and pH in vivo.	[19]
Fluorescent biosensors based on microbial rhodopsin engineered by single point mutation.	Supplemented E. coli. of chloride at physiological pH in exogenously.	Realize reversible readout of chloride in live bacteria.	[20]
X-Ray analytical methods such as X-Ray Fluorescence (XRF) or Energy Dispersive X-Ray Fluorescence (EDS).	SKOV3 ovarian cancer cell and etc. after treatment of chloride channel blocker Furosemide and then freeze-drying.	Enables long-term preservation of samples and enables tricky measurements.	[21]

10. References

1 Y. X. Wang, J. M. Noël, J. Velmurugan, W. Nogala, M. V. Mirkin, C. Lu, M. Guille Collignon, F. Lemaître and C. Amatore, *Proc. Natl. Acad. Sci. U. S. A.*, 2012, **109**, 11534-11539.

2 Y. Li, K. K. Hu, Y. Yu, S. A. Rotenberg, C. Amatore and M. V. Mirkin, *J. Am. Chem. Soc.*, 2017, **139**, 13055-13062.

3 Y. L. Ying, Y. X. Hu, R. Gao, R.-J. Yu, Z. Gu, L. P. Lee and Y.-T. Long, *J. Am. Chem. Soc.*, 2018, **140**, 5385-5392.

4 R. R. Pan, M. C. Xu, J. D. Burgess, D. Jiang and H.-Y. Chen, *Proc. Natl. Acad. Sci. U. S. A.*, 2018, **115**, 4087-4092.

5 X. W. Zhang, A. Oleinick, H. Jiang, Q.-L. Liao, Q.-F. Qiu, I. Svir, Y.-L. Liu, C. Amatore and W.-H. Huang, *Angew. Chem. Int. Ed.*, 2019, **58**, 7753-7756.

6 K. K. Hu, Y. Li, S. A. Rotenberg, C. Amatore and M. V. Mirkin, *J. Am. Chem. Soc.*, 2019, **141**, 4564-4568.

7 Y. F. Ruan, F. Z. Chen, Y. T. Xu, T.-Y. Zhang, S.-Y. Yu, W.-W. Zhao, D. Jiang, H.-Y. Chen and J.-J. Xu, *Angew. Chem. Int. Ed.*, 2021, **60**, 25762-25765.

8 X. Li, Y. Jin, F. H. Zhu, R. Liu, Y. Jiang, Y. Jiang and L. Mao, *Angew. Chem. Int. Ed.*, 2022, **61**, e202208121.

9 A. Fazelkhah, S. Afshar, K. Braasch, M. Butler, E. Salimi, G. Bridges and D. Thomson, *Biotechnol. Bioeng.*, 2019, **116**, 2896-2905.

10 U. Neuhaus Steinmetz, S. Skrandies and L. Rensing, *Brain Res.*, 1996, **724**, 16-24.

11 E. Pozo-Guisado, A. Alvarez-Barrientos, S. Mulero-Navarro, B. Santiago-Josefat and P. M. Fernandez-Salguero, *Biochem. Pharmacol.*, 2002, **64**, 1375-1386.

12 G. Liu, B.-K. Jin, C. Ma, Z. Chen and J.-J. Zhu, *Anal. Chem.*, 2019, **91**, 6363-6370.

13 L. Li, P. Li, J. Fang, Q. Li, H. Xiao, H. Zhou and B. Tang, *Anal Chem*, 2015, **87**, 6057-6063.

14 G. N. Berta, P. Salamone, A. E. Sprio, F. Di Scipio, L. M. Marinos, S. Sapino, M. E. Carlotti, R. Cavalli and F. Di Carlo, *Oral Oncology*, 2010, **46**, 42-48.

15 M. Tsukimoto, H. Harada, A. Ikari and K. Takagi, *J Biol Chem*, 2005, **280**, 2653-2658.

16 Q. Wang, L. Wang, Y.-H. Feng, X. Li, R. Zeng and G. I. Gorodeski, *Am. J. Physiol., Cell Physiol.*, 2004, **287**, C1349-C1358.

17 R. G. Painter and G. Wang, *Anal. Chem.*, 2006, **78**, 3133-3137.

18 H. Chi, Q. Zhou, J. N. Tutol, S. M. Phelps, J. Lee, P. Kapadia, F. Morcos and S. C. Dodani, *ACS Synth. Biol.*, 2022, **11**, 1627-1638.

19 S. Sulis Sato, P. Artoni, S. Landi, O. Cozzolino, R. Parra, E. Pracucci, F. Trovato, J. Szczurkowska, S. Luin, D. Arosio, F. Beltram, L. Cancedda, K. Kaila and G. M. Ratto, *Proc. Natl. Acad. Sci. U. S. A.*, 2017, **114**.

20 S. M. Phelps, J. N. Tutol, D. Advani, W. Peng and S. C. Dodani, *Chem. Commun.*, 2023, **59**, 8460-8463.

21 R. Gunawan, M. Yang and C. Lau, *Talanta Open*, 2023, **7**.